Materials Horizons

Tensile and Torsional Elastomer Fiber Artificial Muscle by Entropic Elasticity with Thermo-Piezoresistive Sensing of Strain and Rotation by Single Electric Signal

Journal:	*Materials Horizons*
Manuscript ID	MH-COM-06-2020-001003.R1
Article Type:	Communication
Date Submitted by the Author:	29-Sep-2020
Complete List of Authors:	Wang, Run ; Nankai University Shen, Yanan; Nankai University Qian, Dong; University of Texas at Dallas, Department of Mechanical Engineering Sun, jinkun; Nankai University Zhou, Xiang; China Pharmaceutical University Wang, Weichao; Nankai University, College of Electronic Informaiton and Optical Engineering Liu, Zun-Feng; State Key Laboratory of Medicinal Chemical Biology, College of Pharmacy, Nankai University, Tianjin, 300071, China,

New concepts:

It is highly desired to develop intelligent soft robotics as smart as mankind by biomimetic ergonomic design. The artificial muscle is one of the key elements for constructing soft robotics. How to mimic the working mechanism and functions of human muscles is still a challenge. Although twisted fibers have been shown to work as powerful artificial muscles, there has not been a concept of integrating the functions of neuron, sensing, and actuation in such artificial muscles. This work provides a new concept of how to realize signal transmission, signal feedback, and actuation in a single fiber, by using a combined structure of fiber twisting and buckle formation of the conducting layer. Such idea of multi-functional design and muscle structure were demonstrated for the first time, whereas previous researches about twisted artificial muscles mainly focus on the actuation performance by modifying the twisted structures. Another novelty in this research is torsional actuation of an elastomer fiber by a mechanism of entropic elasticity, while in previous research only tensile actuation was demonstrated by entropic elasticity. This design strategy for multi-functional artificial muscles would also be applicable for other types of artificial muscles driven by different stimuli.

COMMUNICATION

Tensile and Torsional Elastomer Fiber Artificial Muscle by Entropic Elasticity with Thermo-Piezoresistive Sensing of Strain and Rotation by Single Electric Signal†

Received 00th January 20xx,
Accepted 00th January 20xx

DOI: 10.1039/x0xx00000x

Run Wang,‡[a] Yanan Shen,‡[b] Dong Qian,[c] Jinkun Sun,[b] Xiang Zhou,[d] Weichao Wang[a] and Zunfeng Liu*[ab]

Natural muscles show tensile actuation and realize torsional rotation by combining with skeletons, which integrate with sensing and signaling function in a single element to form a feedback loop. The currently developed artificial muscle and sensing devices always work upon external stimuli, and a separate controlling and signal transmission system is needed, increasing the complexity of muscle design. Therefore it is highly desired to develop flexible and compact fiber artificial muscles with large strain for advanced soft robotic systems. In this paper, twisted elastomer fiber artificial muscles with tensile and torsional actuations and sensing function by single electric signal are developed, by using twisted natural rubber fiber coated with buckled carbon nanotube sheet. The twisted natural rubber fiber can be electrothermally actuated to show contraction and rotation by entropic elasticity. The buckled carbon nanotube sheet can transmit electric current, and the contact area between the buckled carbon nanotube sheets increased during actuation, resulting in resistance decrease by thermo-piezoresistive effect. A feedback circuit was designed to connect or disconnect the electric current by measuring the resistance change to form a feedback loop to control on/off of the muscle. The current study provides new muscle design for soft robotics, controllers, and human-machine integration.

1. Introduction

Natural muscles show tensile actuation and realize torsional rotation by combining with skeletons upon receiving the signals sending from the brain through central neuron systems (Fig. 1). The working mechanism of the human muscle system according to the sliding filament theory is as follows. The signal, an impulse called an action potential, travels through a type of motor neuron, where the motor neuron forms synaptic junctions with either extrafusal muscle fibers (skeletal muscle) or intrafusal fibers (muscle spindle), as shown in Fig. 1a.[1-5] The neuronjunction allows the alpha (α) motor neuron to transmit a signal to the muscle fiber, causing muscle contraction (Fig. 1b). Muscle contraction is generated by the myosin cross-bridges, which interact cyclically with thin actin filaments and transport them to the myosin thick filaments (Fig. 1c). The calcium ions bind to troponin on the actin filaments causing tropomyosin to slide over and unblock the remainder of the actin-binding site. Then the myosin heads close and bind strongly to actin-binding site. The myosin head then releases the inorganic phosphate (Pi) to initiate a power stroke, which generates moving inward of the actin filament, thereby shortening the sarcomere and releasing adenosine diphosphate (ADP). Muscle spindles are skeletal muscle sensory receptors within the body of a muscle that primarily detect length changes of the muscle fibers contributing to gamma (γ) motor control and providing axial and limb position information to the central nervous system (Fig. 1d). The α-γ coordination serves as a rudimentary means of sensorimotor control and plays an important role in governing the human movement and posture. Therefore, it is highly desired to construct such a soft artificial muscle that mimics this natural skeletal muscle and central nervous system for soft robotics.

In recent years, different types of actuators have been designed to realize bending, contraction, and rotation, including bimorph actuators,[6-8] pneumatic actuators,[9-12] dielectric actuators,[13-15] twisted fiber artificial muscles,[16-24] *etc*. The actuation behavior of these muscles was generally obtained by external cameras and image processing systems. Such a sensing system is complex and always not mobile, therefore combining a flexible sensor with artificial muscles is a preferred design. Recently, several important progresses were achieved by attaching a strain sensor onto the actuator to monitor the bending and contraction,[25-31] and a single muscle that can sense the deformation was constructed.[31-35] These artificial muscles use electric signals for sensing, and the information of bending and contractile deformation can be obtained during actuation. However, they always work upon external stimuli such as heat,

[a] State Key Laboratory of Medicinal Chemical Biology, College of Chemistry and College of Electronic Information and Optics Engineering, Key Laboratory of Functional Polymer Materials, Nankai University, Tianjin 300071, China
[b] College of Pharmacy, Nankai University, Tianjin, 300071, China.
[c] Department of Mechanical Engineering, The University of Texas at Dallas, Richardson, TX 75080, USA
[d] Department of Science, China Pharmaceutical University, Nanjing, Jiangsu, 211198, China
*Corresponding author E-mail: liuzunfeng@nankai.edu.cn
‡ These authors contributed equally to this work.
†Electronic Supplementary Information (ESI) available: See
DOI: 10.1039/x0xx00000x

light, compressed air, *etc*, and a separate controlling and signal transmission system is needed. This increases the complexity of the design and control system of the muscles and sensors. Therefore, a single artificial muscle that works on a single electric signal for actuation and self-sensing is highly desired for convenient control.

Moreover, although the artificial muscle materials such as pneumatic actuators, shape memory alloys, dielectric elastomers, and piezoelectric actuators are mature techniques and work well in the robotic systems, these actuators suffer from bulk size (pneumatic), high cost, hysteresis and low strain (shape memory alloy), high electric field (dielectric), and lack of flexibility (piezoelectric actuators).[9, 36-39] Therefore it is highly desired to develop flexible and compact fiber artificial muscles with large strain for advanced soft robotic systems. Twisted fibers are used for tensile and torsional artificial muscles from carbon nanotube yarns and their composites,[16-19] polyethylene and nylon fishing line,[20, 21] silk and cotton yarns,[22, 23] and elastomer fibers by dielectric mechanism.[24] Rubber fibers were used as thermally driven tensile artificial muscles by entropic elasticity. For a rubber fiber extended by loading a weight, heating resulted in contraction of the rubber fiber due to entropic elasticity.[40-42] To the best of our knowledge, torsional artificial muscles for twisted elastomer fibers driven by the entropic elasticity mechanism have not been previously reported.

Recently, coiled bilayer structures using a rigid fiber on a pre-stretched elastomer were prepared to mimic the cucumber tendril and work as powerful tensile artificial muscles [43-46], and a thin layer of silver wire was coated on this tendril muscle to monitor the strain using resistance change.[47] However, self-sensing of the deformation of the twisted fiber actuators was not utilized to prepare a feedback loop to self-control the on/off of the actuators in the above research. Up to now, it has not yet been realized for an artificial muscle that integrates both tensile and torsional actuation by a single electrical signal for stimulation and sensing in a single element, which can self-control the on/off of actuation via a feedback loop by sensing the muscle deformation, by mimicking the natural muscle system.

In this paper, sensing, signalling, and tensile and torsional actuation were realized in a single elastomer fiber artificial muscle by designing a bi-sheath buckled carbon nanotube (CNT) skin on an elastomer fiber core, which was actuated and sensed by a single electrical stimulus (Fig. 1e and 1f). The elastomer fiber acted as a thermally-driven artificial muscle, which contracts due to the entropic elasticity[48-50] by electro-heating of the CNT layer. The entropy of the stretched elastomer was lower than the non-stretched elastomer, and heating the pre-stretched rubber fiber increased its elastic modulus, thereby causing the isobarically loaded elastomer fiber to contract (Fig. 1g, and Fig. S1b, ESI†). The contacting area between the CNT buckles increased during thermally driven contraction of the elastomer fiber, resulting in nearly linear resistance change as a function of strain during electrothermal actuation. Therefore, the muscle length can be monitored by measuring the resistance of the CNT sheath, which was analogous to the length sensing of the human muscle fiber by muscle spindles (Fig. 1h). Moreover, torsional actuation can also be monitored by the thermo-piezoresistance change of the CNT skin layer, for a torsional artificial muscle that was prepared by connecting an elastomer fiber muscle to a return spring followed by twist insertion. A feedback loop was designed to self-control the actuation by sensing the muscle deformation.

2 Results and discussion

2.1 Tensile muscle and resistance change during actuation

The muscle was prepared by using a pre-stretch induced buckling of forest drawn CNT sheets on an elastomer fiber.[24, 30, 51, 52] To increase buckle contacting of the CNT layer, a double-sheath strategy was used here,[53] which was briefly described as follows. A natural rubber fiber was used as the central element of the muscle, which showed good thermal stability (Fig. S1a, ESI†). First, a 2.5-mm-diameter natural rubber fiber was pre-stretched to 600% strain and coated with a thin layer of thermal plastic elastomer (TPE, 100 μm), then the CNT sheets were attached on the surface of the fiber. Dipping a drop of ethanol on CNT increased the interfacial adhesion between CNT and TPE, with CNT alignment direction parallel to the fiber length direction. Releasing the pre-strain of the rubber fiber produced highly-contacting CNT buckles (Fig. 1h). We chose the maximum available strain (600%) as the fabrication strain to ensure that the CNT sheet was not broken when the rubber fiber was loaded by any weight before fracture. The CNT-coated elastomer was labelled as CNT_m/elastomer, where m indicates the number of CNT layers of the CNT sheets. For such a muscle design, the Young's modulus of the natural rubber fiber (1.1 MPa) is much higher than that of the thin TPE layer (46.8 KPa), in order to obtain a large muscle force and negligible influence of the sensing layer to the muscle performance. Stress-strain curves showed that coating CNT and TPE thin layers did not significantly affect the mechanical properties of the natural rubber fiber (Fig. S1b, ESI†). The CNT_m/elastomer showed increased resistance with stretching (Fig. S2, ESI†), and we observed decreased buckle contacting upon stretching the CNT_m/elastomer (Fig. S3, ESI†).

A stretched elastomer tends to contract when it is heated, due to the well-known entropic elasticity of elastomers.[48-50] As the CNT_m/elastomer fiber is a typical elastic conductor, it can be heated by using direct current. The first electro-thermal actuation experiment was carried out on a CNT_m/elastomer fiber isobarically-loaded with constant stress, which showed contractile actuation upon electric power supply (Fig. 2a). We first investigated the dependence of electric voltage on the muscle performance. Increasing the applied voltage increased the electric power and the muscle temperature, and at the same time we observed increased tensile stroke (Fig. 2c and Fig. S5a, ESI†). The input electric work was calculated by integration of applied current over time during electrothermal actuation, which was normalized to the initial length of the CNT_m/elastomer fiber. The tensile stroke was defined as $\Delta L/L$, where L and ΔL are the instantaneous length (loaded length)

and the length decrease of the muscle fiber. For a CNT_{10}/elastomer fiber muscle with an initial length of 7.0 cm and isobaric stress of 0.8 MPa, as the voltage increased from 0 to 150 V, the electric power increased from 0 to 0.7 W/cm, the muscle temperature increased from 21 to 125°C, and the tensile stroke increased from 0% to 23.2%. The work capacity evaluates how much work the muscle can do per unit mass. The work capacity of the CNT_{10}/elastomer muscle increased almost linearly from 0 to 0.54 kJ/kg as the electric power increased from 0 to 0.7 W/cm, and increasing the number of CNT layers negligibly affected the dependence of output work capacity on the input electric power (Fig. 2c).

We then investigated the dependence of the tensile stroke on the isobaric load. The tensile stroke of the CNT_{10}/elastomer muscle increased first from 0% to reach a maximum value of 23.2% as the isobaric stress increased from 0 to 0.8 MPa, and then decreased to 10.0% as the isobaric stress further increased to 2.0 MPa (Fig. 2d). As the instantaneous length of the elastomer increased dramatically with increasing the isobaric load, we then define an apparent tensile stroke ($\Delta l/l_o$) relative to the initial length (l_o) to evaluate the contracted length of the muscle. This apparent tensile stroke is much higher than the tensile stroke relative to the instantaneous length. For the CNT_{10}/elastomer muscle driven at 0.7 W/cm electric power, the apparent tensile stroke increased from 0% to 68.6% as the isobaric load increased from 0 to 1.0 MPa, reached a plateau as the isobaric load increased to 1.4 MPa, and decreased as the isobaric load further increased (Fig. S5b, ESI†). A similar dependence of the apparent tensile stroke on isobaric load was observed for the electric power of 0.31 and 0.48 W/cm. The maximum measured contractile work capacity increased from 0.71 to 1.06 kJ/kg as the load increased from 1.0 to 1.6 MPa and reached a plateau as the isobaric load further increased (Fig. S6a, ESI†), which is over 20 times as that of natural human muscles (~0.04 kJ/kg).[21] The maximum energy conversion efficiency was 0.5% based on the input electrical energy and output mechanical work during the electro-thermal actuation (Fig. S6b, ESI†). Additionally, the performances of the CNT_m/elastomer muscles were compared with the artificial muscles based on other elastomer materials, including dielectric elastomers, liquid crystal elastomers, and rubber elastomers, as shown in Table S1.

Increasing the number of CNT layers decreased the resistance of the CNT_m/elastomer, which would decrease the required electric voltage to obtain the same heating power. The CNT_m/elastomer showed resistance increase upon stretching, and the percent resistance change with percent strain decreased with increasing the number of CNT layers (Fig. 2e). The CNT_m layer serves as both electro heating and strain sensing by resistance change. Fig. 2e shows the percent resistance change for the CNT_m/elastomer fiber under stretch, increasing the number of layers resulted in decreased percent resistance change. So a too large *m* resulted in low value of the percent resistance change, meaning a low sensitivity of strain sensing. While a too small *m* resulted in very high electric voltage needed to thermally drive the CNT_m/elastomer muscle. Therefore, in the actuation experiments in Fig. 2b, we chose moderate *m* values (10 and 20), rather than a too small value (3) or a too big value (50), in order to obtain reasonable resistance change for actuation driven by a reasonable voltage. Figure 2e inset shows that there is no degradation in performance after 1000 stretch/release cycles. Moreover, figure S4 shows the relative resistance change of the CNT_{10}/elastomer at various strain rates under 110% strain, and no strain rate dependence for the electrical response is observed for stretch rate ranging from 2 to 55 mm/s. While the resistance quasi-linearly changed upon stretching below 100% strain, this piezoresistive characterization is carried out at room temperature. This does not reflect the real situation of the resistance change during electrothermal actuation of the CNT_m/elastomer muscle, where the muscle temperature would also affect the resistance.

We then measured the resistance of a CNT_{10}/elastomer muscle upon electro-heating at different isobaric stress (Fig. 2f and Fig. S7, ESI†). It can be seen that the resistance of a CNT_{10}/elastomer muscle isobarically loaded with 0.8 MPa stress quasi-linearly decreased from 1.74 to 1.60 kΩ as the muscle was electro-thermally actuated from a length of 8.1 to 6.7 cm. We also observed similar quasi-linear resistance change during electro-thermal actuation of the muscle when it was elongated to a larger length when loaded with a heavier weight (1.5 MPa) (Fig. S7, ESI†). Such a quasi-linear piezoresistive effect during actuation would provide the CNT_m/elastomer muscle the possibility of obtaining the muscle length by measuring the resistance.

We then investigated if the electro-heating contributed to the resistance change during actuation of the CNT_m/elastomer muscle. The CNT_{10}/elastomer muscle was extended by 140%, which was the same as the length as it was isobarically loaded with 0.6 MPa stress (Fig. 2g). Then the muscle was electro-heated by applying a voltage of 45 V with both-end tethered (isometrically). It is discovered that the resistance of the CNT_{10}/elastomer fiber decreased by 11.3% (from 1.67 to 1.48 kΩ during isometric heating for 30 s, which is slightly smaller than that (12.0%, from 1.67 to 1.47 kΩ) during isobaric heating to allow muscle contraction. This indicates that heating-induced buckle contact should be an important contribution to the resistance decrease during actuation, which can be nominated as thermo-piezoresistive effect and has been investigated in detail in our previous research.[54]

2.2 Torsional elastomer muscle and resistance change

Besides contraction, human muscles also show torsional actuation by combining with skeletons. Although the heat-induced contraction is well known for elastomers, thermally driven torsional actuation of elastomers has not been realized so far. One way to prepare torsional artificial muscle is to insert twist into fibers, and volume expansion of the fiber results in twist release and torsional rotation.[16-18, 20-22, 24] In this section,

we investigated the fabrication and characterization of torsional elastomer muscles by inserting twist into the CNT_m/elastomer fibers.

We first evaluated the effect of twist insertion on the tensile stroke of the CNT_m/elastomer muscle. A 2.5-mm-diameter CNT_m/elastomer muscle was isobarically loaded with a weight, and twist was inserted in the muscle fiber while the load was torsionally tethered. As twist insertion increased the length of the elastomer muscle fiber when it is isobarically loaded with a stress, in order to obtain the same the muscle length before actuation, the load was decreased with an increase in the inserted twist. The tensile stroke monotonically decreased with increasing the twist density until fiber coiling (Fig. 2h, and Fig. S8, ESI†). As the twist density increased from 0 to 4.3 turns/cm, the tensile stroke decreased from 19.3% to 2.1% for an isometric strain of 160%, and decreased from 9.1% to 1.8% for an isometric strain of 60%. The tensile stroke almost kept a constant value by increasing the twist density from coil initiation to fully coiling. An interesting point of this CNT_m/elastomer muscle is that its tensile stroke is constant by inserting twist at different strains (Fig. S9, ESI†), which would provide stable contracting performance when twist insertion was carried out at different lengths.

The above experiments showed that simply inserting twist did not realize torsional actuation, while it decreased the tensile stroke of the CNT_m/elastomer muscle. In order to obtain torsional actuation, we connected a thin elastomer fiber (1.5 mm in diameter) in between the CNT_m/elastomer and the load, and attached a thin paddle on the joint of the two elastomer fibers. By torsionally tethering the load and inserting twist from the top side, more twist was inserted into this thin elastomer fiber compared to the CNT_m/elastomer fiber, which served as the twist reservoir. As the CNT_m/elastomer was subjected to electro-heating, we observed untwisting of the CNT_m/elastomer and torsional rotation of the paddle, indicating that twist was transferred from the CNT_m/elastomer to the thin fiber. At the same time, we observed contractile actuation of the CNT_m/elastomer. This should be originated from the increase in torsional stiffness in CNT_m/elastomer fiber under heating. The theoretical explanation for torsional actuation of CNT_m/elastomer fiber was shown in Supplementary Section S1 (ESI†).

The torsional stroke of the torsional muscle was defined as the rotational angle divided by the instantaneous length of the CNT_m/elastomer fiber. The torsional stroke increased monotonically from 0 to 87.6 degree/cm as the twist density increased from 0 to 1.6 turns/cm, and at the same time it was observed that the tensile stroke of the CNT_{10}/elastomer slightly decreased from 19.4% to 16.0% (Fig. 3b). Decreasing the muscle diameter allowed us to insert more twists into the muscle fiber, and as a result the torsional stroke increased accordingly. At the same time the diameter of the thin elastomer fiber used as the return spring also decreased accordingly. The torsional stroke of a 0.6-mm-diameter CNT_{10}/elastomer fiber increased from 0 to a maximum value of 364.0 degree/cm as the twist density increased from 0 to 5.0 turns/cm, and then slightly decreased to 328.0 degree/cm as the twist density further increased to 6.0 turns/cm. The tensile stroke of this 0.6-mm-diameter CNT_{10}/elastomer muscle slightly decreased from 18.0% to 16.0% as the twist density increased from 0 to 6 turns/cm. We then investigated how the torsional stroke correlated with tensile stroke as the muscle was driven at different electrical power (Fig. 3c). As the electrical power increased from 0 to 0.7 W/cm, the torsional stroke, tensile stroke, and actuating temperature almost linearly increased from 0 to 82.6 degree/cm, from 0% to 16.2%, and from 21 to 125°C, respectively; and a nearly linear correlation was observed for the tensile stroke and torsional stroke (Fig. 3c, inset).

Fiber plying is always used in textile industry to obtain scalability and stability during twist insertion. We next investigated how plying affected the torsional and tensile actuation of the torsional CNT_m/elastomer muscles. Two identical torsional muscles composed of a 2.5-mm-diameter CNT_{10}/elastomer and a thin elastomer fiber (1.5 mm in diameter) were plied together, while it was isobarically loaded with 0.4 MPa weight and torsionally tethered. With increasing the twist density from 0 to 0.7 turns/cm, the torsional stroke increased from 0 to 50.8 degree/cm and almost reached a plateau, and the tensile stroke slightly decreased from 15.0% to 14.3% (Fig. 3d). The torsional stroke, tensile stroke, and temperature also almost linearly increased with an increase of the electrical power, and the torsional stroke linearly increased with tensile stroke (Fig. 3e), which was similar to the case of the single-ply muscle. As a large diameter fiber needed less twist to reach the same bias angle than a small diameter fiber, we then normalized the two-ply and single-ply muscles to the same bias angle by multiplying the twist density and the fiber diameter to obtain an equivalent inserted twist (Fig. S10, ESI†). The equivalent diameter of the two-ply muscle was obtained using the total area of the cross-sections of the two individual fibers as the cross-sectional area of an equivalent thicker fiber. The dependence of the torsional stroke on the equivalent inserted twist below 0.2 turns was almost the same for the single-ply and two-ply torsional muscles. This indicated the scalability of this torsional muscle by fiber plying for at low twist region.

Although entropic elasticity driven contraction of elastomers upon heating is known for hundreds of years, torsional actuation of elastomers based on entropic elasticity has not been reported so far. The above experiments showed that torsional actuation occurred accompanying with contractile actuation upon electro heating of the twisted CNT_{10}/elastomer fiber, when it was connected to a twist reservoir. In this section, we investigated how the resistance change for the torsional CNT_m/elastomer muscle during such heating-induced tensile and torsional actuations. On applying 0.35 W/cm of electric power to a torsional CNT_{10}/elastomer muscle with inserted twist of 1.7 turns/cm, the muscle temperature increased by 75°C in 35 s, at the same time the paddle rotated by 38.6 degree/cm, the CNT_{10}/elastomer contracted by 8.9%, and the resistance increased by 9.1% (Fig. 3f). Increasing the voltage resulted in higher heating rate and larger rotational and tensile strokes. In order to show the correlation of resistance change with torsional and tensile actuations, we plotted the torsional and tensile strokes as a

function of resistance change (Fig. 3g and Fig. S11, ESI†). It can be seen that torsional and tensile strokes monotonically increased with an increase in percent resistance change. The tensile and torsional strokes have unique correlation with resistance change for different applied voltages, which should be derived from different temperatures arising from electro-heating. The maximum-obtained muscle temperatures at 45, 55, and 65 V voltage were 75, 100, and 125°C, respectively. This also provided us the possibility of obtaining the temperature of the muscle from the curve profiles between the actuation stroke and the percent resistance change.

The CNT_m/elastomer muscle is consisted of buckled CNT sheet on the rubber fiber surface. There are two parameters affecting the resistance of the CNT sheet. (1) The CNT buckles contacted at relaxed state, and the contacting extent of the buckles decreased as the length of the CNT_m/elastomer muscle increased, resulting in resistance increase; it is vice versa for the reversal process, *i.e.* the buckle contact increased as the length of the CNT_m/elastomer muscle decreased, resulting in resistance decrease. This was observed in Fig. 2f in this paper, as well as in our previous study of bi-sheath buckled strain sensor.[53] (2) For a CNT_m/elastomer muscle, an increase in the rubber temperature resulted in increased buckle contact due to thermal expansion of the rubber fiber as well as the buckled thin rubber layer in between the CNT sheet and the rubber fiber, resulting in resistance decrease. This heating induced resistance decrease was observed in Fig. 2g in this study, as well as in our previous study about bi-sheath buckled temperature sensor[54]. Therefore, the combination of the above piezoresistive effect and negative thermoresistive effect would produce resistance decrease during heating induced contraction of the CNT_m/elastomer muscle.

It is interesting that for the self-sensing CNT_m/elastomer muscle, electro-heating of the muscle produced temperature increase. This temperature increase caused length decrease and stiffness increase of the CNT_m/elastomer muscle, which further caused untwist of the CNT_m/elastomer muscle when it was connected with a return spring followed by twist insertion to make a torsional artificial muscle. This untwist of the CNT_m/elastomer muscle actually decreased the spiral length of the muscle fiber and should also result in decreased resistance. Because the temperature, length, and twist are closely related to each other during actuation, measuring the resistance of the CNT_m/elastomer muscle can provide information of temperature, length, and twist.

2.3 A self-controlling muscle by the feedback loop

Natural muscle has a protection mechanism: it releases the actuation force when the lifted weight exceeds its maximum loading capacity. Here we designed a feedback loop to realize such a self-controlling artificial muscle. During electro-heating induced contraction of the CNT_m/elastomer muscle, we observed monotonic resistance decrease. We then designed a computational algorithm to control the electric circuit using resistance. As the resistance reached a low critical value during muscle contraction, the electric circuit was disconnected; and during muscle length recovery the circuit re-connected again as the resistance reached a high critical value (Fig. 4a). The experiment was carried out on a tensile artificial muscle prepared from a 2.5-mm-diameter CNT_{10}/elastomer fiber isobarically loaded with 0.6 MPa stress. As a result, we observed repeated muscle contraction and extension accompanying with resistance decrease and increase, respectively (Fig. 4b). Figure 4c-f shows that as the resistance increased to a value of 1.03 kΩ, the electric circuit connected automatically (the indicator light went out) and the muscle started to contract; and as the resistance decreased to a value of 1.01 kΩ, the electric circuit dis-connected automatically (the indicator light burning) and the muscle started to elongate. Our constructed CNT_m/elastomer artificial muscle can be actuated and sensed by a single electric stimulus, which is different from those artificial muscles responded by external stimulus that needed a separate actuation sensing system for controlling (Table S2). Moreover, the feedback loop for self-sensing and controlling the muscle actuation would provide a possible way for preparing self-adaptive muscles used for controllers, switches, and robotics.

Therefore, we developed a prototype of a soft walking robot that can crawl with a worm-like motion. The soft robot, composed of a pre-strained CNT_{10}/elastomer muscle and curved polypropylene film (Fig. 4g), was actuated with electrical stimuli on a ratchet substrate. As the power was on, the rear leg slid forward while the front leg was prevented from sliding backward. Similarly as the power was off, the front leg slid forward with the rear leg constrained by the ratchet surface (Fig. 4g). As a result, the repeated bending and unbending motions of the two legs can be converted into forward motion (Fig. 4h and 4i). The connection and disconnection of the electric circuit automatically switched using the above algorithm by measuring the resistance change of the CNT_{10}/elastomer muscle, resulting in autonomous crawling of the soft robot.

2.4 Theoretical section for the tensile and torsional actuations

The thermoelastic response of the rubber is governed by the entropic elasticity theory, which assumes that the macroscopic response of the rubber is due to the changes in the conformational states of the polymer chain rather than the stretch of the chains themselves. Neglecting the latter, the free energy is given as[55]

$$F = \frac{3}{2} k_B T \frac{D^2}{Nb^2} + const \qquad (1),$$

in which k_B is Boltzmann constant, *T* is temperature, *D* is end-to-end distance of the chain, *N* is the number of segments in the chain with segment length *b*. eqn. (1) assumes a simple monomer polymer chain model. Based on this, one can show that both the stress σ and elastic stiffness E are linearly proportional to temperature T, as shown in Fig. S1B (ESI†).

We developed a theoretical model to explain the observed dependence of tensile stroke on applied stress. Following eqn. (1), we introduce a 2-term Mooney-Rivlin rubber elasticity model, given as

$$\sigma = \left(\lambda - \frac{1}{\lambda^2}\right)\left(C_1 + \frac{C_2}{\lambda}\right)T \qquad (2),$$

in which σ is the applied isobaric stress defined as the load divided by the initial cross-sectional area, λ is the stretch ratio, given as the ratio of the elongated length over the initial length, C_1, C_2 are two constants obtained from fitting eqn. (2) to the measured stress-strain curve, T is inherited from the entropic elasticity model as mentioned above.

We assume thermal equilibrium in the actuated state so that the supplied electric work W is the same as the heat loss from the rubber to the surrounding air. Assuming constant supplied electric work W, it can be shown that

$$\sqrt{\lambda}\left(\frac{T}{T_0} - 1\right) = \frac{W}{2h\pi r_0 l_0} \qquad (3),$$

with h as the convective heat transfer coefficient, r_0 and l_0 are respectively the initial radius and length of the rubber. The expressions for temperature T and T_0 in eqn. (3) can be analytically obtained from eqn. (2). After substitution into eqn. (3), a nonlinear equation of λ as a function of the initial stretch at λ_0 room temperature is obtained. This nonlinear equation is solved numerically to get λ, which is then substituted into eqn. (2) to obtain the stress for each applied electric power. The tensile stroke can be converted from the stretch ratio. Combining the results gives the stress dependence of the tensile stroke as shown in Fig. 2d.

We next provide a theoretical model for the torsional CNT$_m$/elastomer muscle. In an important report, it was developed a theoretical model for torsional actuation of twisted, thermally-set nylon torsional muscles, which provided a theoretical free torsional rotation angle without the influence of return spring.[56] As the torsional CNT$_m$/elastomer muscle was not thermally set, the inserted twist would be totally released if the thin elastomer fiber (return spring) was absent. Therefore, the observed untwist in heated torsional CNT$_m$/elastomer muscle can be explained by the following theoretical model (see Supplementary Section S1 for detailed calculations, ESI†).

Since the fibers were torsionally tethered at both ends after twist insertion and thermal activation, the total twist remained unchanged. As mentioned in section 2.2, the CNT$_m$/elastomer fiber was first connected to a thin elastomer fiber and then twist was inserted. The total twist can be given as θ. We consider the torque balance before the application of the heat. We use $k_1$and k_2 to represent the torsional stiffness of the CNT$_m$/elastomer fiber and thin elastomer fiber, respectively. After the heat is applied, k_1 increases to k_1'. Based on the calculation details in Supplementary Section S1 (ESI†), the twist angle change ($\Delta\theta_1$) of the CNT$_m$/elastomer fiber can be given as

$$\Delta\theta_1 = \frac{k_1' - k_1 \quad k_2}{k_1' + k_2 k_1 + k_2}\theta \qquad (4).$$

Fig. S12 (ESI†) compares the experimentally measured torsional actuation and prediction using eqn. (4). A good agreement is observed for the dependence of the torsional actuation on the twist density. This remarkable agreement was expected due to the linear elasticity assumption of the elastomer fiber employed in the theoretical model and a low twist range of the experiment.

3 Conclusions

In this paper, an artificial muscle that combines functions of actuation, controlling, sensing, and signal transmission in a single muscle element was fabricated by mimicking the natural muscle and neuron functions. This was realized by assembling a carbon nanotube sheath with contacted buckles on an elastomer fiber. The elastomer fiber can be electro-thermally actuated via a mechanism of entropic elasticity. The carbon nanotube sheath served as an electric current transmission pathway for electro-thermal actuation of the muscle. The resistance of the buckled carbon nanotube layer decreased monotonically during electro-thermal actuation, which was used to monitor the muscle length, and the resistance signal also transmitted through the carbon nanotube sheath. A torsional elastic muscle based on an entropic elasticity mechanism was also fabricated for the first time. This was realized by inserting twist into a carbon nanotube coated elastomer fiber that was connected to a thin elastomer fiber. Both torsional and tensile actuation can be monitored by measuring the resistance change. A feedback loop was further designed to automatically connect and disconnect the electrical circuit of the muscle by setting an upper and a lower resistance limit. The current research provides new design strategies of multi-functional artificial muscles for switches, controllers, and soft robotics.

4 Material and methods

4.1 Fabrication of tensile and torsional CNT$_m$/elastomer muscles

The tensile CNT$_m$/elastomer muscle was prepared using a pre-strain strategy. First, a natural rubber fiber (Zhixin Rubber Products Co. Ltd.) was prestretched to 600% strain, then a thin layer (100 μm in thickness) of thermal plastic elastomer (styrene-ethylene-butylene-styrene copolymer mixed with liquid wax by a mass ratio of 1:5). Next, forest-drawn carbon nanotube sheets (produced by chemical vapor deposition method[52]) were attached on this thin layer of thermal plastic elastomer, followed by dipping of a drop of ethanol. After ethanol evaporation, the pre-strain of the natural rubber was released to produce a CNT$_m$/elastomer fiber, which can be directly used as an electro-thermally driven tensile muscle when it was isobarically loaded with a weight. Unless otherwise indicated, the CNT$_m$/elastomer muscles were 2.5 mm in diameter and 7.0 cm long in a relaxed state.

To prepare a torsional muscle, the above-prepared CNT$_m$/elastomer fiber was connected to a thin elastomer fiber, and a load was hanged at the bottom side of this thin elastomer fiber. Then twist was inserted from the topside of the CNT$_m$/elastomer using an 80-step server motor, while the load was torsionally tethered to avoid twist release. Then a paddle was attached at the joint site of the CNT$_m$/elastomer and the thin fiber. The torsional return spring (made of similar latex rubber as the actuating segment) was also two-ply and comprised individual fibers that were 1.5 mm in diameter and 4.5 cm long.

4.2 Scanning electron microscope (SEM), electrical and actuation characterizations, thermal gravimetric analysis (TGA), and mechanical analysis

For actuation, the muscles were electro-heated by connecting two thin copper wires to the top end and the bottom end of the CNT_m/elastomer, and voltage was applied using a Keithley 2400 source meter. An infrared meter was used to obtain the tensile actuation, a video camera was used to obtain the torsional actuation stroke by analyzing the videos, the resistance was obtained from the Keithley 2400 source meter, and the temperature was obtained from a thermo-camera (FLIR T440).

The SEM images of the CNT_m/elastomer were obtained on Nova NanoSEM450 field emission scanning electron microscope. The thermogravimetric analysis was obtained on a thermogravimetric analyzer (Netzsch model TG209F3) in N_2 atmosphere. The stress-strain curves were obtained on Instron 5566 machine at a strain rate of 5 mm/min. The torsional stiffness (k) of the CNT_m/elastomer fiber and the thin rubber fiber (return spring) was measured by a torsion pendulum technique (Fig. S12a inset, ESI†), where a needle placed in the middle point of fiber was subjected to small angular displacement to result in harmonic motion. The period (t) of the needle was used to calculate the torsional stiffness of the CNT_m/elastomer fiber and thin rubber fiber through the eqn. (7).

$$t = 2\pi\sqrt{\frac{I}{k}} \qquad (7),$$

in which I is the moment of inertia of the needle.

Appendix A. Supplementary data

Supplementary data to this article can be found online.

Authorship Contributions

R.W., Y.S., and Z.L. conceived and initiated the project. All authors contributed to experimental design, planning, and execution; data analysis, and manuscript writing, D.Q. contributed to the theoretical model.

Conflicts of interest

There are no conflicts to declare.

Acknowledgements

R. W. and Y. S. contributed equally to this work. This work was supported by the National Key Research and Development Program of China (grant 2016YFA0200200, grant 2017YFB0307001), the National Natural Science Foundation of China (grants 51973093, U1533122, and 51773094), the Natural Science Foundation of Tianjin (grant number 18JCZDJC36800), National Special Support Plan for High-level Talents people (grant number C041800902), the Science Foundation for Distinguished Young Scholars of Tianjin (grant number 18JCJQJC46600), the Fundamental Research Funds for the Central Universities (grant 63171219), and State Key Laboratory for Modification of Chemical Fibers and Polymer Materials, Donghua University (grant LK1704). The US National Science Foundation (grant CMMI 1727960). We thank Wuhan Zeal Young Technology Co., Ltd. for software programming.

References

1. E. N. Marieb and K. Hoehn, *Human Anatomy & Physiology*, Pearson education, 2007.
2. R. G. Dennis and H. Herr, in *Biomimetics*, CRC Press, 2005, pp. 261-284.
3. G. A. Bekey, *Autonomous Robots: from Biological Inspiration to Implementation and Control*, MIT press, London, England, 2005.
4. L. Ricotti and A. Menciassi, *Biomed. Microdevices*, 2012, **14**, 987-998.
5. J. C. Dean, *Exerc. Sport Sci. Rev.*, 2013, **41**, 36.
6. J. Li, R. Zhang, L. Mou, M. Jung de Andrade, X. Hu, K. Yu, J. Sun, T. Jia, Y. Dou, H. Chen, S. Fang, D. Qian and Z. Liu, *Adv. Funct. Mater.*, 2019, **29**, 1808995.
7. Y. Hu, G. Wu, T. Lan, J. Zhao, Y. Liu and W. Chen, *Adv. Mater.*, 2015, **27**, 7867-7873.
8. J. Mu, C. Hou, H. Wang, Y. Li, Q. Zhang and M. Zhu, *Sci. Adv.*, 2015, **1**, e1500533.
9. F. Daerden and D. Lefeber, *E. J. Mech. Environ. Eng.*, 2002, **47**, 11-21.
10. D. Saravanakumar, B. Mohan and T. Muthuramalingam, *Precis. Eng.*, 2017, **49**, 481-492.
11. M. A. Robertson, H. Sadeghi, J. M. Florez and J. Paik, *Soft Robot.*, 2017, **4**, 23-32.
12. S. Terryn, J. Brancart, D. Lefeber, G. Van Assche and B. Vanderborght, *Sci. Robot.*, 2017, **2**, 1-12.
13. C. Löwe, X. Zhang and G. Kovacs, *Adv. Eng. Mater.*, 2005, **7**, 361-367.
14. L. J. Romasanta, M. A. López-Manchado and R. Verdejo, *Prog. Polym. Sci.*, 2015, **51**, 188-211.
15. H. Godaba, J. Li, Y. Wang and J. Zhu, *IEEE Robot. Autom. Lett.*, 2016, **1**, 624-631.
16. J. Foroughi, G. M. Spinks, G. G. Wallace, J. Oh, M. E. Kozlov, S. Fang, T. Mirfakhrai, J. D. Madden, M. K. Shin, S. J. Kim and R. H. Baughman, *Science*, 2011, **334**, 494-497.
17. M. D. Lima, N. Li, M. J. De Andrade, S. Fang, J. Oh, G. M. Spinks, M. E. Kozlov, C. S. Haines, D. Suh, J. Foroughi, S. J. Kim, Y. Chen, T. Ware, M. K. Shin, L. D. Machado, A. F. Fonseca, J. D. W. Madden, W. E. Voit, D. S. Galvão and R. H. Baughman, *Science*, 2012, **338**, 928-932.
18. J. Mu, M. J. De Andrade, S. Fang, X. Wang, E. Gao, N. Li, S. H. Kim, H. Wang, C. Hou, Q. Zhang, M. Zhu, D. Qian, H. Lu, D. Kongahage, S. Talebian, J. Foroughi, G. Spinks, H. Kim, T. H. Ware, H. J. Sim, D. Y. Lee, Y. Jang, S. J. Kim and R. H. Baughman, *Science*, 2019, **365**, 150-155.
19. S. Aziz and G. M. Spinks, *Mater. Horizons*, 2020, 667-693.
20. C. S. Haines, M. D. Lima, N. Li, G. M. Spinks, J. Foroughi, J. D. Madden, S. H. Kim, S. Fang, M. J. De Andrade, F. Göktepe, Ö. Göktepe, S. M. Mirvakili, S. Naficy, X. Lepró, J. Oh, M. E. Kozlov, S. J. Kim, X. Xu, B. J. Swedlove, G. G. Wallace and R. H. Baughman, *Science*, 2014, **343**, 868-872.

21. C. S. Haines, N. Li, G. M. Spinks, A. E. Aliev, J. Di and R. H. Baughman, *P. Natl. Acad. Sci. USA*, 2016, **113**, 11709-11716.
22. T. Jia, Y. Wang, Y. Dou, Y. Li, M. Jung de Andrade, R. Wang, S. Fang, J. Li, Z. Yu, R. Qiao, Z. Liu, Y. Cheng, Y. Su, M. Minary‐Jolandan, R. H. Baughman, D. Qian and Z. Liu, *Adv. Funct. Mater.*, 2019, **29**, 1808241.
23. Y. Li, X. Leng, J. Sun, X. Zhou, W. Wu, H. Chen and Z. Liu, *Chin. Phys. B*, 2020, **29**, 048103.
24. Z. Liu, S. Fang, F. Moura, J. Ding, N. Jiang, J. Di, M. Zhang, X. Lepró, D. Galvao, C. Haines, N. Y. Yuan, S. G. Yin, D. W. Lee, R. Wang, H. Y. Wang, W. Lv, C. Dong, R. C. Zhang, M. J. Chen, Q. Yin, Y. T. Chong, R. Zhang, X. Wang, M. D. Lima, R. Ovalle-Robles, D. Qian, H. Lu and R. H. Baughman, *Science*, 2015, **349**, 400-404.
25. J. C. Yeo, H. K. Yap, W. Xi, Z. Wang, C. H. Yeow and C. T. Lim, *Adv. Mater. Technol.*, 2016, **1**, 1600018.
26. H.-P. Phan, T. Dinh, T.-K. Nguyen, A. Vatani, A. R. Md Foisal, A. Qamar, A. R. Kermany, D. V. Dao and N.-T. Nguyen, *Appl. Phys. Lett.*, 2017, **110**, 144101.
27. H. Zhao, K. O'Brien, S. Li and R. F. Shepherd, *Sci. Robot.*, 2016, **1**, eaai7529.
28. J. C. Case, E. L. White and R. K. Kramer, *Smart Mater. Struct.*, 2016, **25**, 045018.
29. M. Amjadi and M. Sitti, *Adv. Sci.*, 2018, **5**, 1800239.
30. H. Wang, Z. Liu, J. Ding, X. Lepró, S. Fang, N. Jiang, N. Yuan, R. Wang, Q. Yin, W. Lv, Z. Liu, M. Zhang, R. Ovalle‐Robles, K. Inoue, S. Yin and R. H. Baughman, *Adv. Mater.*, 2016, **28**, 4998-5007.
31. H. Cheng, F. Zhao, J. Xue, G. Shi, L. Jiang and L. Qu, *ACS Nano*, 2016, **10**, 9529-9535.
32. T. A. Gisby, B. M. O'Brien and I. A. Anderson, *Appl. Phys. Lett.*, 2013, **102**, 193703.
33. S. Rosset, B. M. O'Brien, T. Gisby, D. Xu, H. R. Shea and I. A. Anderson, *Smart Mater. Struct.*, 2013, **22**, 104018.
34. X. Q. Wang, K. H. Chan, Y. Cheng, T. Ding, T. Li, S. Achavananthadith, S. Ahmet, J. S. Ho and G. W. Ho, *Adv. Mater.*, 2020, **32**, 2000351.
35. K. Kruusamäe, P. Brunetto, S. Graziani, A. Punning, G. Di Pasquale and A. Aabloo, *Polym. Int.*, 2010, **59**, 300-304.
36. J. Zhang, J. Sheng, C. T. O'Neill, C. J. Walsh, R. J. Wood, J.-H. Ryu, J. P. Desai and M. C. Yip, *IEEE Trans. Robot.*, 2019, **35**, 761-781.
37. U. Gupta, L. Qin, Y. Wang, H. Godaba and J. Zhu, *Smart Mater. Struct.*, 2019, **28**, 103002.
38. S. Derby, M. Sreekumar, T. Nagarajan, M. Singaperumal, M. Zoppi and R. Molfino, *Ind. Robot.*, 2007, **34**, 285.
39. R. Changhai and S. Lining, *Sensor Actuat. A-Phys*, 2005, **122**, 124-130.
40. J.-H. Jeong, T. J. Mun, H. Kim, J. H. Moon, D. W. Lee, R. H. Baughman and S. J. Kim, *Nanoscale Adv.*, 2019, **1**, 965-968.
41. J. Foroughi, G. M. Spinks, S. Aziz, A. Mirabedini, A. Jeiranikhameneh, G. G. Wallace, M. E. Kozlov and R. H. Baughman, *ACS Nano*, 2016, **10**, 9129-9135.
42. P.-J. Cottinet, D. Guyomar, J. Galineau and G. Sebald, *Sensor Actuat. A-Phys*, 2012, **180**, 105-112.
43. M. Godinho, J. Canejo, G. Feio and E. Terentjev, *Soft Matter*, 2010, **6**, 5965-5970.
44. M. Godinho, J. Canejo, L. Pinto, J. Borges and P. Teixeira, *Soft Matter*, 2009, **5**, 2772-2776.
45. S. J. Gerbode, J. R. Puzey, A. G. McCormick and L. Mahadevan, *Science*, 2012, **337**, 1087-1091.
46. Y. Cheng, R. Wang, K. H. Chan, X. Lu, J. Sun and G. W. Ho, *ACS Nano*, 2018, **12**, 3898-3907.
47. M. Kanik, S. Orguc, G. Varnavides, J. Kim, T. Benavides, D. Gonzalez, T. Akintilo, C. C. Tasan, A. P. Chandrakasan and Y. Fink, *Science*, 2019, **365**, 145-150.
48. H. M. James and E. Guth, *J. Chem. Phys.*, 1943, **11**, 455-481.
49. A. E. Green and W. Zerna, *Theoretical Elasticity*, Courier Corporation, New York, 1992.
50. G. Holzapfel and J. Simo, *Comput. Methods. Appl. Mech. Eng.*, 1996, **132**, 17-44.
51. R. Wang, Z. Liu, G. Wan, T. Jia, C. Zhang, X. Wang, M. Zhang, D. Qian, M. J. de Andrade, S. Yin, R. Zhang, D. Feng, W. Wang, H. Zhang, H. Chen, Y. Wang, R. Ovalle-Robles, K. Inoue, H. Lu, S. Fang, R. H. Baughman and Z. Liu, *ACS Appl. Mater. Inter.*, 2019, **11**, 10862-10873.
52. M. Zhang, S. Fang, A. A. Zakhidov, S. B. Lee, A. E. Aliev, C. D. Williams, K. R. Atkinson and R. H. Baughman, *Science*, 2005, **309**, 1215-1219.
53. R. Wang, N. Jiang, J. Su, Q. Yin, Y. Zhang, Z. Liu, H. Lin, F. A. Moura, N. Yuan, S. Roth, R. Ovalle‐Robles, K. Inoue, S. Yin, S. Fang, W. Wang, J. Ding, L. Shi, R. H. Baughman and Z. Liu, *Adv. Funct. Mater.*, 2017, **27**, 1702134.
54. K. Wu, Z. Liu, H. Lin, R. Wang, Q. Yin, W. Lv, J. Su, N. Yuan, J. Qiu and J. Ding, *J. Nanosci. Nanotechno.*, 2018, **18**, 2732-2737.
55. L. R. G. Treloar, *The physics of rubber elasticity*, Oxford University Press, USA, 1975.
56. S. Aziz, S. Naficy, J. Foroughi, H. R. Brown and G. M. Spinks, *Polym. Test*, 2015, **46**, 88-97.

COMMUNICATION

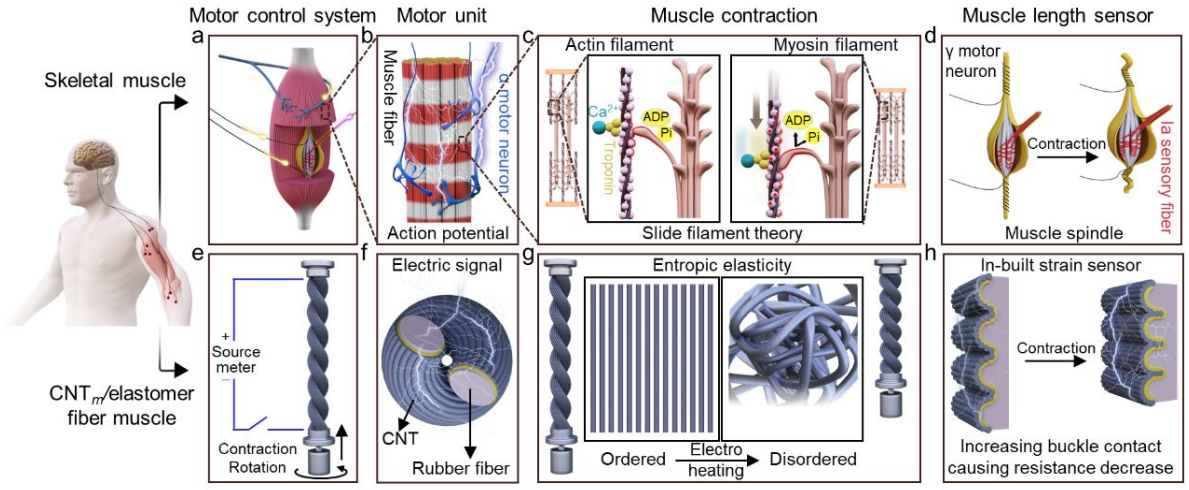

Fig. 1 Schematic illustration of an artificial muscle mimicking the natural skeletal muscle and neuron system that integrates actuation, sensing, signal transmission, and controlling. (a) Motor neuron fibers innervating extrafusal and intrafusal muscle fibers. (b) The extrafusal muscle fibers are innervated by alpha (α) motor neuron, and the neuromuscular junction allows the α motor neuron to transmit the action potential signal to the muscle fibers, causing muscle contraction. (c) The role of calcium, actin, and myosin in muscle contraction. The calcium binds to troponin, exposing myosin binding sites, and then myosin heads bind to an actin filament, and later, a power stroke causes the actin filament to move. (d) A muscle spindle is a proprioceptor, with gamma motor neuron and Ia sensory fibers, that primarily detect muscle length changes contributing to fine motor control and providing position information to the central nervous system. (e) A schematic demonstration of feedback electric circuit can be realized by measuring the resistance change during electro-thermal tensile and torsional actuation of a CNT_m/elastomer muscle. (f) The top view of CNT_m/elastomer muscle. (g) Schematic representation of the macroscopic and molecular mechanism of the electro-thermally induced actuation. (h) During electro-heating induced contractile actuation, the contacting extent between buckles increases, resulting in decreased resistance, which serves as a strain sensor to measure the muscle length during actuation.

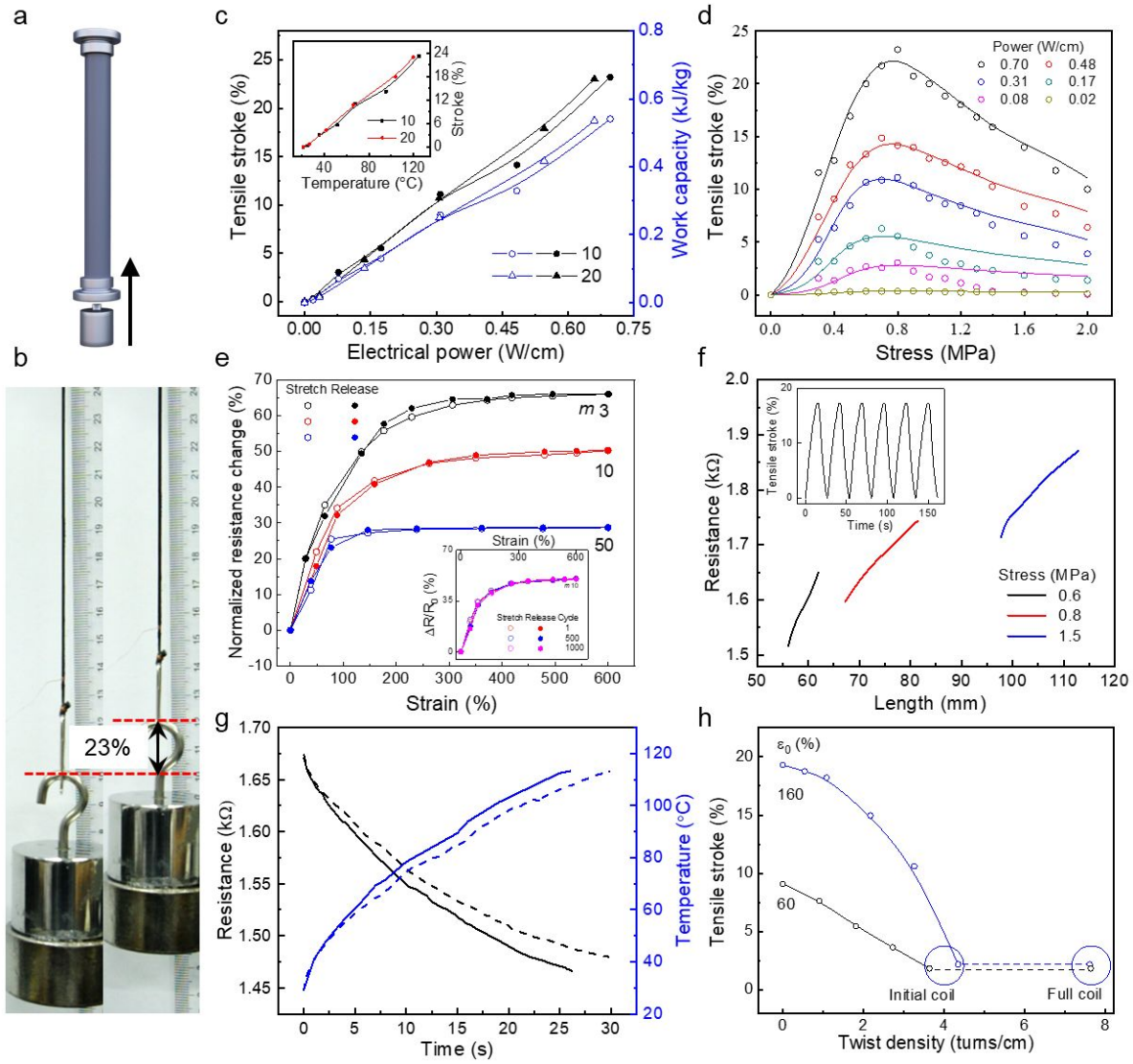

Fig. 2 Electro-thermal tensile actuation and resistance change. (a) Schematic illustration of electro-thermal tensile actuation of a CNT_m/elastomer muscle. (b) Photographs showing a tensile CNT_{10}/elastomer muscle contracted by 23% on applying 0.7 W/cm of electrical power and isobarically loaded with 0.8 MPa stress. (c) Tensile stroke and work capacity as a function of applied electric power for CNT_m/elastomer muscles at isobaric stress of 0.8 MPa (m=10 and 20). The inset in (c) shows the tensile stroke as a function of temperature. (d) Tensile stroke of a CNT_{10}/elastomer muscle as a function of isobaric stress under different electric power, where open circles and solid lines are experimental data and theoretical results, respectively. (e) The percent resistance change of CNT_m/elastomer muscles as a function of applied strain (m=3, 10, and 50). The inset shows the resistance change versus strain for CNT_{10}/elastomer for the indicated number of cycles. (f) Resistance as a function of muscle length for the tensile CNT_{10}/elastomer muscle during electro-thermal actuation at 45 V voltage under different isobaric stress. The inset shows the tensile stroke as a function of time during cyclic actuation. (g) Resistance and temperature as a function of time for the tensile CNT_{10}/elastomer muscle during electro-thermal actuation at 45 V voltage under isobaric load of 0.6 MPa and isometric strain of 140% (equals to the room-temperature muscle length of isobaric load of 0.6 MPa). (h) Tensile stroke for a tensile CNT_{10}/elastomer muscle as a function of inserted twist on applying 0.62 W/cm of electrical power at different initial muscle elongation (ε_0 = 160% and 60%). The initial muscle length is the same for different inserted twist.

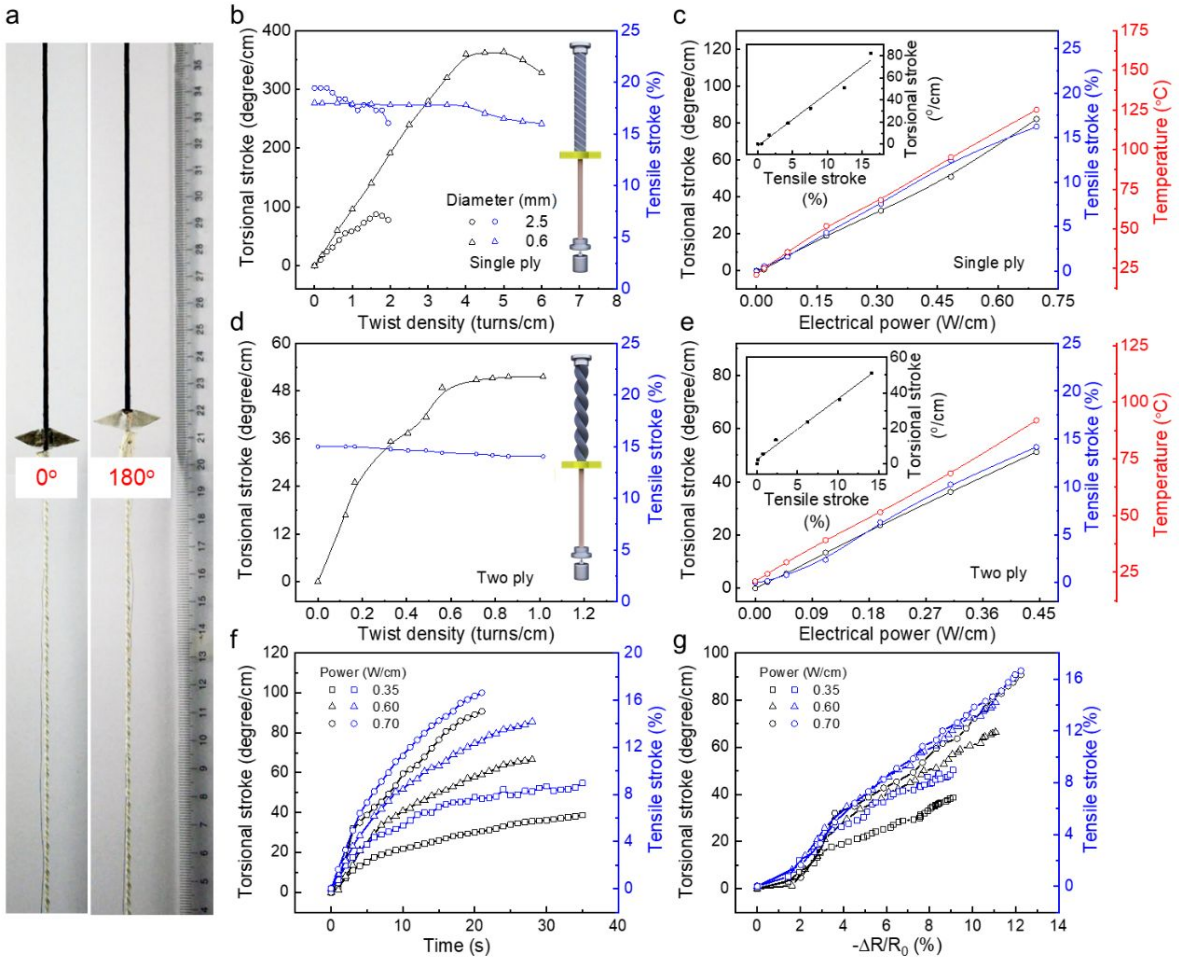

Fig. 3 Electro-thermal torsional actuation and resistance change. (a) Photographs showing the paddle rotates by 180° during electro-thermal actuation of a torsional CNT_{10}/elastomer muscle. (b) Torsional stroke and tensile stroke as a function of twist density for a single-ply torsional CNT_{10}/elastomer muscle with different diameters. (c) Torsional stroke, tensile stroke, and temperature as a function of electric power for a single-ply torsional CNT_{10}/elastomer muscle. The inset shows the dependence of torsional stroke on the tensile stroke. (d) Torsional stroke and tensile stroke as a function of twist density for a two-ply torsional CNT_{10}/elastomer muscle with diameter of 2.5 mm. (e) Torsional stroke, tensile stroke, and temperature as a function of electric power for a two-ply torsional CNT_{10}/elastomer muscle. The inset shows the dependence of torsional stroke on the tensile stroke. (f, g) Torsional, tensile actuation as a function of time (e) and as a function of resistance change (f) for a single-ply torsional CNT_{10}/elastomer muscle during electro-thermal actuation at different electric power under isobaric load of 0.8 MPa. The non-loaded muscle diameter for (a) to (g) is 2.5 mm.

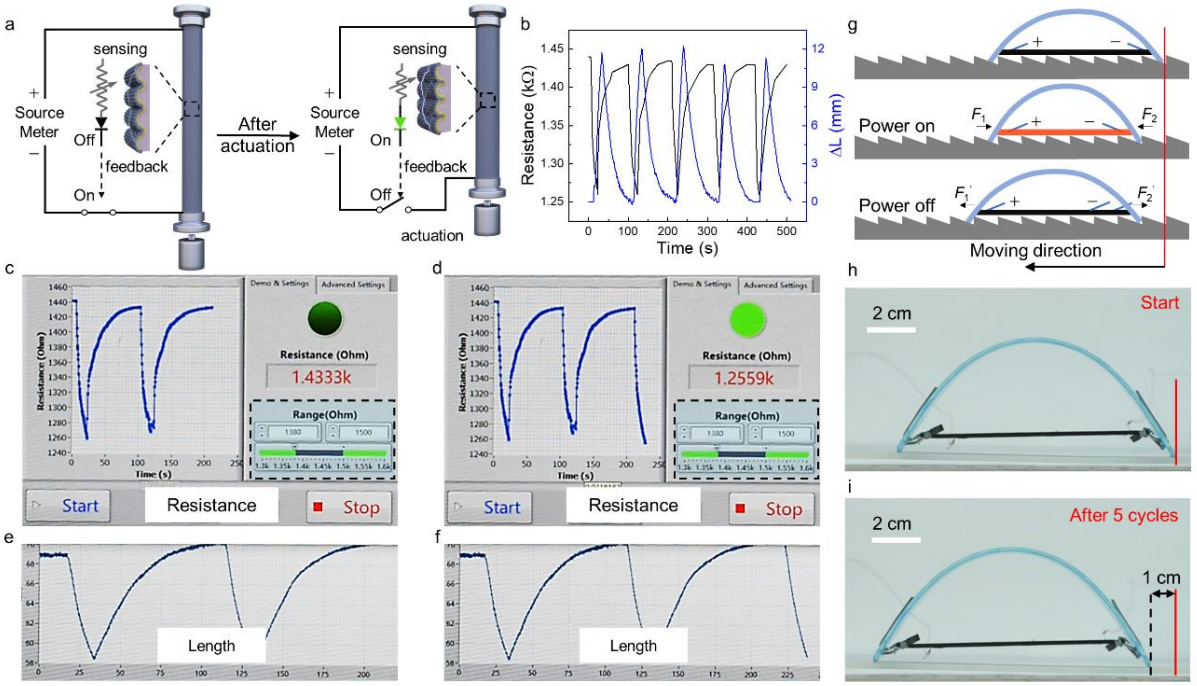

Fig. 4 Demonstration of application of a CNT_m/elastomer muscle as a self-controlled muscle and a soft walking robot. (a) Schematic illustration of a feedback loop of a self-controlled muscle. The electric circuit is connected and the muscle starts to contract when the resistance reaches a low critical value; and the circuit is disconnected and the muscle elongates when the resistance reaches a high critical value. (b) Resistance and muscle length of a tensile CNT_{10}/elastomer muscle as a function of time during the self-controlled connection and disconnection of the circuit. (c-f) Screenshot images showing the lower and upper limits of the resistance and muscle length. the light burning as the resistance reached a minimum value (c) indicated that the electric circuit was disconnected and the muscle started to elongate (e); The light going out as the resistance reached a minimum value (d) indicated that the electric circuit was connected and the muscle started to contract (f). (g) Schematic illustration of the crawling processes and the force analysis in one driving cycle. (h and i) Photographs showing a walking robot crawling forward on a ratchet substrate.